A Performance Analysis of an All-Optical Clock Extraction Circuit Based on Fabry–Perot Filter

Xiang Zhou, *Member, IEEE*, Chao Lu, *Member, IEEE*, Ping Shum, *Member, IEEE*, Hossam H. M. Shalaby, *Senior Member, IEEE*, T. H. Cheng, *Member, IEEE*, and Peida Ye, *Fellow, IEEE*

***Abstract*—A performance analysis of an optical clock extraction circuit based on a Fabry–Perot filter (FPF) is presented. Two analytical methods, time-domain and frequency-domain analysis, are developed in this paper. Time-domain analysis shows that there is no phase jitter in the extracted optical clock if the free spectral range (FSR) of the FPF is exactly equal to the signal clock frequency. Based on this, we obtain an analytical expression for root mean square (rms) amplitude jitter of the extracted optical clock in time domain, in which we have taken the impacts of carrier frequency drift and carrier phase noise into account. When the FSR of the FPF deviates from the signal clock frequency, both phase jitter and amplitude jitter will occur in the extracted optical clock. In this situation, a more general frequency-domain method is developed to deal with the timing performance under the assumption that carrier phase noise is negligible. This method allows us to calculate both rms phase jitter and rms amplitude jitter of the extracted optical clock. Using the developed two methods, we present a detailed numerical investigation on the impacts of finesse of the FPF, carrier frequency drift, resonator detuning, carrier phase noise, and optical pulse chirp on the timing performance. Finally, the application of this circuit in multiwavelength clock recovery is discussed.**

***Index Terms*—Amplitude jitter, Fabry–Perot filter (FPF), multiwavelength clock extraction, optical clock extraction, optical tank circuit, phase jitter.**

I. Introduction

SYSTEM synchronization is one of the serious problems in constructing all-optical signal-processing systems, such as all-optical regenerative repeaters, all-optical time-division switching systems, and all-optical demultiplexers. In order to realize the system synchronization, an all-optical clock extraction circuit, which recovers timing information from an incoming optical data stream and produces an optical clock without an intermediate electric stage, is required.

Up to the present, several optical timing extraction techniques suitable for high-speed operation have been demonstrated. Some examples include inject-locking of a mode-locked laser [1]–[3], optical phase-lock loop (PLL) [4], [5], optical passive tank circuit based on Fabry–Perot filter (FPF) [6], [7], and optical active tank circuit based on stimulated Brillouim scattering (SBS) [8]–[11]. Each of these methods has advantages and drawbacks. For the mode-locked laser, high-quality clock can be recovered. However, when setting up the laser, the cavity length must be tuned carefully. For optical PLL, extremely stable operation is obtainable but such a technique is very complex and more suitable for clock extraction at the frame rate. An optical active tank circuit based on SBS has the unique ability to recover clock in optical domain without knowing the incoming data bit rate. But this technique is still rather complex, and the extracted clock quality is worse than that obtained by both mode-locked laser and optical PLL. Compared with the above-mentioned three optical clock extraction techniques, an optical passive tank circuit based on FPF has the advantages of ultra-high-speed operation (operational speed is considered to be nearly unlimited [7]) and simple configuration due to its passive structure. Moreover, such a technique can also be used for multiwavelength clock recovery, as will be shown in Section IV.

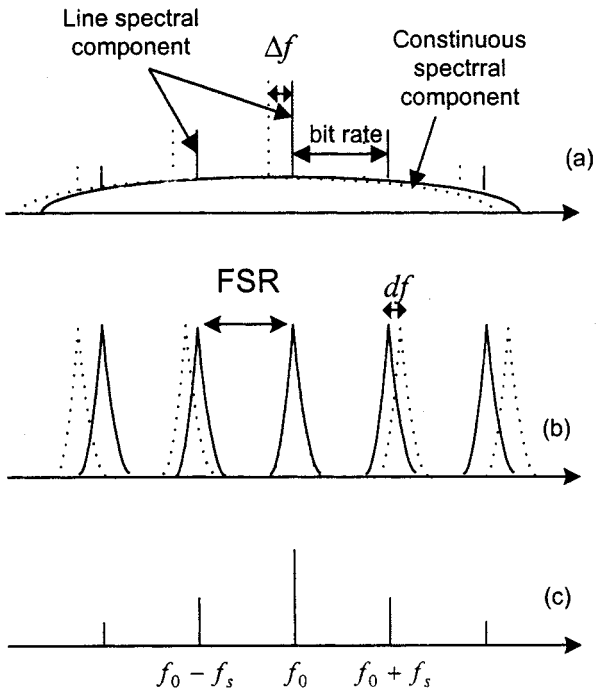

Fig. 1. Principle of the passive optical tank circuit based on a FPF. (a) Optical spectrum of an incoming RZ optical data. (b) Filtering characteristics of the FPF. (c) Optical spectrum of the extracted optical clock (noise is neglected). The dashed lines in (a) denote the case with carrier frequency drift. The dashed lines in (b) correspond to the case with resonator detuning.

The principle of a passive optical tank circuit based on a FPF is shown in Fig. 1. An optical signal created by return-to-zero (RZ) intensity modulation consists of continuous spectral component and line spectral components, i.e., the optical carrier fre-

Manuscript received March 8, 2000; revised January 19, 2001.

X. Zhou, C. Lu, P. Shum, H. H. M. Shalaby, and T. H. Cheng are with the School of Electrical and Electronic Engineering, Nanyang Technological University, Singapore 639798, Singapore (e-mail: ezhoux@ntu.edu.sg).

P. Ye is with Optical Communications Center, Beijing University of Posts and Telecommunications, Beijing 100876, China.

Publisher Item Identifier S 0733-8724(01)03635-0.

quency f_0 and the AM side bands $f_0 \pm f_s$, $f_0 \pm 2f_s \ldots$, where f_s denotes the data clock frequency. All-optical timing extraction can be achieved through extracting these line spectral components with a periodic optical filter such as FPF. FPF has periodic power transmission peaks over a range of optical frequencies, as shown in Fig. 1(b). The peak interval, which is called free spectral range (FSR), is given by the inverse of the round-trip time of the optical resonator. From Fig. 1, we can find if 1) $f_0 = q$FSR (q is an integer), 2) FSR$= f_s$, and 3) the source linewidth is narrower than the resonator bandwidth. Only the line spectral components, which contain the carrier frequency f_0 and the timing components $f_0 \pm f_s$, are transmitted. This results in optical timing clock extraction. In practice, both f_0 and FSR may deviate from the ideal setting due to temperature fluctuations in the optical source and the FPF, and thus cause detuning of the optical tank circuit (for convenience, we define the deviation of f_0 from qFSR as carrier frequency drift and the deviation of FSR from f_s as resonator detuning). In addition, carrier phase noise and optical pulse frequency chirp may also degrade the timing performance. In this paper, we present an analytical study on the timing performance of an all-optical clock extraction circuit based on FPF. In our analysis, we have considered the effects of carrier frequency drift, resonator detuning, carrier phase noise, and optical pulse chirp. To our knowledge, this is the first time this issue is being dealt with.

The remainder of this paper is organized as follows. Section II is devoted to time-domain analysis. An analytical expression for root mean square (rms) amplitude jitter of the extracted optical clock under the assumption that there is no resonator detuning is achieved. A more general method to deal with the timing performance is derived in Section III, in which we have taken both carrier frequency drift and resonator detuning into account. In Section IV, we present some numerical results, where we investigate the effects of some parameters (finesse of the FPF, carrier frequency drift, resonator detuning, carrier phase noise, and optical pulse chirp) on the timing performance of the passive optical tank circuit. The application of this circuit in multiwavelength clock recovery is also discussed in this section. Finally, we give our conclusions in Section V.

II. Time-Domain Analysis

Recall that a FPF consists of two parallel highly reflective mirrors (see Fig. 2), in which a light ray enters the resonator structure and then rebounds inside the cavity until all its power is transmitted forward or backward (ignoring absorption). At the output, the rays can interfere constructively or destructively. Let $e_i(t)$ and $e_0(t)$ represent the input and output fields of the FPF, respectively. $e_0(t)$ is given by

$$e_o(t) = T \sum_{k=o}^{\infty} e_i(t - kT_R) R^k \tag{1}$$

where T_R means the transmission delay between the two mirrors ($T_R = 1/\text{FSR}$) and T and R denote the transmissivity and the reflectivity of the filter, respectively. For an RZ intensity-modulated optical data stream, $e_i(t)$ is given by

$$e_i(t) = \sum_{n=-\infty}^{\infty} a_n u(t - nT_s) e^{j2\pi f_o t + \phi(t)}. \tag{2}$$

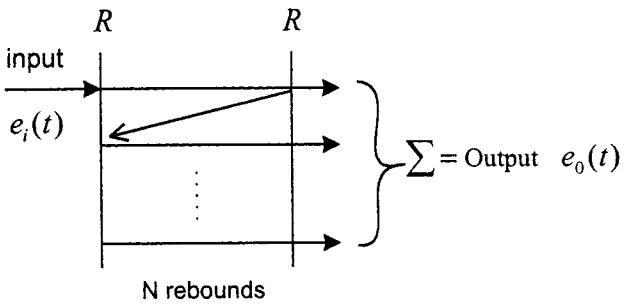

Fig. 2. Basic behavior of a Fabry–Perot filter.

In (2), T_s is the data clock period; a_n takes the unipolar values zero or one with equal probability in the interval $[nT_s, (n+1)T_s]$; and f_0, $\phi(t)$, and $u(t)$ represent the center frequency of the carrier, the phase noise, and the complex envelope of the optical pulse, respectively. Then we can rewrite the transmitted field $e_0(t)$ as

$$e_o(t) = T \sum_{k=0}^{\infty} \sum_{n=-\infty}^{\infty} a_n u(t - nT_s - kT_R) R^k \cdot e^{j2\pi f_o (t - kT_R) + \phi(t - kT_R)}. \tag{3}$$

For an ideal clock extraction, we have FSR$= f_s$, $f_0 = q$FSR (q is an integer) and $\phi(t) \approx 0$. In this situation, $e_0(t)$ can be expressed as

$$e_o(t) = T e^{j2\pi f_0 t} \sum_{m=-\infty}^{\infty} b_m u(t - mT_s)$$
$$b_m = \sum_{k=0}^{\infty} a_{m-k} R^k. \tag{4}$$

From (4), it is clear that there is only amplitude jitter in the extracted optical clock.

Now let us consider the case that FSR$= f_s$, $f_0 \neq q$FSR, and $\phi(t) \neq 0$. In this situation, f_0 can be expressed as

$$f_0 = qFSR + \Delta f \qquad (0 < |\Delta f| < \text{FSR}/2) \tag{5}$$

where Δf is defined as the carrier frequency drift. Substituting (5) into (3), we can express $e_0(t)$ as

$$e_0(t) = \sum_{m=-\infty}^{\infty} b_m(t) u[t - mT_s]$$
$$b_m(t) = T e^{j2\pi f_0 t} \sum_{k=0}^{\infty} a_{m-k} R^k e^{j[-2\pi \Delta f k T_s + \phi(t - kT_s)]}. \tag{6}$$

It is obvious that there is still no phase jitter in the extracted optical clock.

Finally, we consider the case that FSR$\neq f_S$. From (3), the field of the extracted optical clock pulse in the interval $[nT_s, (n+1)T_s]$ can be given by

$$T \sum_{k=0}^{\infty} a_{n-k} u(t - nT_s - k(T_R - T_s)) R^k e^{j2\pi f_o (t - kT_R) + \phi(t - kT_R)}.$$

It is easily seen that both amplitude jitter and phase jitter will occur in the extracted optical clock.

From the above discussion, we can see that so long as FSR$=f_s$, there is only amplitude jitter in the extracted optical clock. In this situation, time-domain method can be directly utilized to obtain the analytical expression for rms amplitude jitter of the extracted optical clock. From (6), the optical intensity of the extracted optical clock is given by

$$I_0(t)=\sum_{m=-\infty}^{\infty}|b_m(t)|^2|u(t-mT_s)|^2 \tag{7}$$

$$|b_m(t)|^2=T^2\sum_{k_1=0}^{\infty}\sum_{k_2=0}^{\infty}a_{m-k_1}a_{m-k_2}R^{k_1+k_2}\cdot e^{j[-2\pi\Delta fT_s(k_1-k_2)+\phi_{k_1k_2}]} \tag{8}$$

$$\phi_{k_1k_2}=\phi(t-k_1T_s)-\phi(t-k_2T_s). \tag{9}$$

Note that (9) corresponds to Gaussian probability density function, which is only dependent on carrier linewidth δf and the value of $|k_1-k_2|T_s$ [12]. We can easily observe that for various values of t and m, $|b_m(t)|^2$ should have the same probability density function. Therefore, we can directly write the normalized rms amplitude jitter of the extracted optical clock as

$$\sigma_A=\frac{\sqrt{\langle|b_m(t)|^4\rangle-\{\langle|b_m(t)|^2\rangle\}^2}}{\langle|b_m(t)|^2\rangle} \tag{10}$$

where $\langle\ \rangle$ means statistical average. For the case that a_n takes the unipolar values zero and one with equal probability, $\langle|b_m(t)|^2\rangle$ can be given as

$$\langle|b_m(t)|^2\rangle=\frac{1}{4}T^2\left[2\frac{1}{1-R^2}+\frac{1}{1-R^2}\frac{2.R.e^a\cos b-2R^2e^{2a}}{1-2.R.e^a\cos b+R^2e^{2a}}\right] \tag{11}$$

where $a=-\pi\delta fT_s$ and $b=2\pi\Delta fT_s$. $\langle|b_m(t)|^4\rangle$ is given by

$$\begin{aligned}\langle|b_m(t)|^4\rangle=&\frac{1}{16}T^4\left\{\left(\frac{1}{1-R^2}\right)^2\left[\frac{1-R^2e^{2a}}{1-2Re^a\cos b+R^2e^{2a}}\right]^2\right.\\&\left.+\left(\frac{2}{1-R^2}\right)\frac{1-R^2e^{2a}}{1-2Re^a\cos b+R^2e^{2a}}\right\}\\&+\frac{1}{8}T^4\left\{\frac{1}{1-R^4}\left[\frac{2R^{2(1+a)}}{1-R^{2(1+a)}}+1\right]\right.\\&+\frac{2A\cos b-2R^2}{(1+R^2-2A\cos b)(1-B^2)}\\&\left.\cdot\left[\frac{1}{1-R^2}-\frac{B^2}{1-R^2B^2}\right]+\frac{R^2}{(1-R^2)(1-R^4)}\right.\\&\left.\cdot\left[\frac{2A\cos b-2R^2}{1+R^2-2A\cos b}-\frac{2AR^2\cos b-2R^6}{1+A^2R^4-2R^2A\cos b}\right]\right.\\&\left.+\frac{A^4}{1-A^2}\frac{2B\cos b-2R^4}{1-2A^2B\cos 2b+A^2R^4}\frac{1}{1-R^4}\right\}\\&+\frac{1}{8}T^4\Re\left\{\frac{1}{(1-BD)^2}\right.\\&\left.\cdot\left[\frac{1}{1-(AC)^2}\frac{2BD}{1-A^2BC}+\frac{(BD)^2}{1-A^2B^2}\right]\right.\\&\left.+\frac{11}{(1-AD)^2}\frac{(AD)^2}{1-A^2B^2}+\frac{2}{1-BD}\right.\\&\left.\cdot\left[\frac{AD}{1-R^2CA}-\frac{ABD^2}{1-R^2AB}\right]\right\}\\&+\frac{1}{16}T^4\left\{\left(\frac{1}{1-R^2}\right)^2+\frac{1}{1-R^4}\right.\\&\left.\cdot\left[\frac{2.R^{2(1+a)}}{1-R^{2(1+a)}}+1\right]\right\}\\&+\frac{1}{16}T^4\Re\left\{\frac{2A^2C^2}{1-(AC)^2(1-R^2)}+\frac{1}{1-R^4}\right\}\\&-\frac{1}{8}T^4\frac{1}{1-R^4}\end{aligned} \tag{12}$$

where $A=Re^a$, $B=Re^{-a}$, $C=e^{jb}$, $D=e^{-jb}$, and $\Re\{h\}$ means the real part of $\{h\}$. The deduction process of (12) is given in Appendix A. Thus, based on (10)–(12), the value of σ_A can be obtained. For an ideal clock extraction, we have $A=R$, $B=R$, $C=1$, and $D=1$. σ_A is then reduced to

$$\sigma_A=\sqrt{\frac{3}{2}-R-\frac{R^2}{2}-\frac{1}{2}\frac{(1-R^2)(1-R)^2}{1+R^2}}. \tag{13}$$

III. Frequency-Domain Analysis

In the previous section, we showed that both amplitude and phase jitter will occur in the extracted optical clock if FSR$\neq f_S$. In this situation, it is difficult to investigate the statistical properties of the extracted optical clock directly by time-domain method. In this section, we will develop a more general frequency-domain method to deal with it.

A. RMS Phase Jitter

Assuming that the carrier phase noise is negligible (i.e., $\delta f\approx 0$), we can use $E_i(t)$ and $E_0(t)$ to represent the baseband form of the input and output data optical fields of the FPF, respectively. The baseband form of the frequency transfer function of the FPF can be expressed as

$$H(f)=\sum_{k=-\infty}^{\infty}H_0(f-kf_s-kdf+\Delta f) \tag{14}$$

where

$$H_0(f)=\begin{cases}\dfrac{1-R}{1-R.e^{j2\pi f/\mathrm{FSR}}}, & |f|\le\dfrac{\mathrm{FSR}}{2}\\ 0, & \text{else.}\end{cases} \tag{15}$$

Δf denotes the carrier frequency drift and df denotes the resonator detuning defined as $df=\mathrm{FSR}-f_s$. Thus $E_0(t)$ can be expressed as

$$\begin{aligned}E_0(t)&=\sum_{k=-\infty}^{\infty}E_i(t)\otimes\left(h_0(t)e^{j2\pi(kf_s+kdf-\Delta f)t}\right)\\&=\sum_{k=-\infty}^{\infty}B_k(t)e^{j2\pi kf_st+j\theta_k(t)}.\end{aligned} \tag{16}$$

In (16), $h_0(t)$ is the temporal response of $H_0(f)$, $\otimes$ denotes convolution integration, and $B_k(t)$ and $\theta_k(t)$ are real random functions. We consider the case that the optical pulse chirp in the incoming data pulse is relatively small and the pulse is not too narrow. In this case, the phase of the extracted optical clock

is mainly dependent on the three terms of $k = 0$, 1, and -1 in (16), and the contribution of other higher order harmonics to clock phase becomes negligible. Thus we can take $E_0(t)$ as

$$E_0(t) = B_0(t)e^{j\theta_0(t)} + B_1(t)e^{j(2\pi f_s t+\theta_1(t))} + B_{-1}(t)e^{-j(2\pi f_s t-\theta_{-1}(t))}. \quad (17)$$

Mathematically, we can write $B_0(t)$, $B_1(t)$, $B_{-1}(t)$, $\theta_0(t)$, $\theta_1(t)$, and $\theta_{-1}(t)$ as $B_1(t) = B_1 + \Delta B_1(t)$, $B_0(t) = B_0 + \Delta B_0(t)$, $B_{-1}(t) = B_{-1} + \Delta B_{-1}(t)$, $\theta_1(t) = \theta_1 + \Delta\theta_1(t)$, $\theta_0(t) = \theta_0 + \Delta\theta_0(t)$, and $\theta_{-1}(t) = \theta_{-1} + \Delta\theta_{-1}(t)$, where B_1, B_0, B_{-1}, θ_1, θ_0, and θ_{-1} are the statistical average of $B_1(t)$, $B_0(t)$, $B_{-1}(t)$, $\theta_1(t)$, $\theta_0(t)$, and $\theta_{-1}(t)$, respectively. In general cases, we should have $B_1 \gg \Delta B_1(t)$, $B_0 \gg \Delta B_0(t)$, $B_{-1} \gg \Delta B_{-1}(t)$, $B_1 \approx B_{-1}$, and

$$\cos\left(\frac{\theta_1(t)+\theta_{-1}(t)}{2} - \theta_0(t)\right) \approx 1.$$

Consequently, the corresponding optical intensity $|E_0(t)|^2$ can be given by

$$|E_0(t)|^2 = \left[B_0 + 2B_1\cos\left(2\pi f_s t + \frac{\theta_1(t)-\theta_{-1}(t)}{2}\right)\right]^2 + \text{small term}. \quad (18)$$

It can be easily seen that $[\theta_1(t) - \theta_{-1}(t)]/2$ just characterizes the phase of the extracted optical clock. Thus, we can write the normalized rms phase jitter of the extracted optical clock as

$$\sigma_J = \frac{1}{4\pi}\sqrt{\langle[\Delta\theta_1(t) - \Delta\theta_{-1}(t)]^2\rangle}. \quad (19)$$

From (16) and (17), we get

$$B_1(t)\cos(2\pi f_s t + \Delta\theta_1(t)) = \Re\left\{\left(E_i(t)\otimes\left(h_0(t)e^{j2\pi(f_s+df-\Delta f)t}\right)\right)e^{-j\theta_1}\right\} \quad (20)$$

$$B_{-1}(t)\cos(2\pi f_s t - \Delta\theta_{-1}(t)) = \Re\left\{\left(E_i(t)\otimes\left(h_0(t)e^{-j2\pi(f_s+df+\Delta f)t}\right)\right)e^{j\theta_{-1}}\right\}. \quad (21)$$

At time $t_n = (2n+1)/(4f_s)$ where n is an integer, we have

$$B_1(t_n)\sin(\Delta\theta_1(t_n)) = \Re\left\{\left(E_i(t)\otimes\left(h_0(t)e^{j2\pi(f_s+df-\Delta f)t}\right)\right)e^{-j\theta_1}\right\}_{t=t_n} \quad (22)$$

$$B_{-1}(t_n)\sin(\Delta\theta_{-1}(t_n)) = \Re\left\{\left(E_i(t)\otimes\left(h_0(t)e^{-j2\pi(f_s+df+\Delta f)t}\right)\right)e^{j\theta_{-1}}\right\}_{t=t_n}. \quad (23)$$

Note that $\Delta\theta_1(t_n)$ and $\Delta\theta_{-1}(t_n)$ are very small. It is clear that $\sin(\Delta\theta_1(t_n)) \approx \Delta\theta_1(t_n)$ and $\sin(\Delta\theta_{-1}(t_n)) \approx \Delta\theta_{-1}(t_n)$. In addition, we can take $B_1(t_n) \approx B_1$ and $B_{-1}(t_n) \approx B_{-1}$. Then we get (24), as shown at the bottom of the page, where

$$\begin{aligned}
Q_1(f) &= U(f)H_0(f - f_s - df + \Delta f)\\
Q_{-1}(f) &= U(f)H_0(f + f_s + \Delta f + df)\\
P_1(f) &= Q_1(f)\otimes Q_1(f)\\
P_{-1}(f) &= Q_{-1}(f)\otimes Q_{-1}(f)\\
PP_1(f) &= Q_1(f)\otimes Q_1^*(-f)\\
PP_{-1}(f) &= Q_{-1}(f)\otimes Q_{-1}^*(-f)\\
PQ(f) &= Q_1(f)\otimes Q_{-1}(f)\\
PG(f) &= Q_1(f)\otimes Q_{-1}^*(-f)\\
\vartheta_1 &= \arg[P_1(2f_s)], \qquad \vartheta_{-1} = \arg[P_{-1}(2f_s)]\\
\varphi_q &= \arg[PQ(0)], \qquad \varphi_G = \arg[PG(2f_s)]
\end{aligned}$$

where $U(f)$ is the Fourier transform of $u(t)$ and $\arg[h]$ means the argument of $[h]$.

B. RMS Amplitude Jitter

Considering both the phase and amplitude jitter, we can write the extracted optical clock (in the optical intensity form) in a general form as

$$I_c(t) = [1 + a(t)]\sum_{n=-\infty}^{\infty} g(t - nT_s - J(t)) \quad (25)$$

where $a(t)$, $J(t)$, and $g(t)$ denote the normalized optical intensity variation, the timing fluctuation, and the average optical clock pulse intensity envelope, respectively. The power spectral density of $I_c(t)$ can be approximately given as [13], [14]

$$S_I(f) \cong f_s^2\sum_{n=-\infty}^{\infty}|G(nf_s)|^2[S_a(f - nf_s) + 4\pi^2 n^2 f_s^2 S_J(f - nf_s) + \delta(f - nf_s)]. \quad (26)$$

In (26), $G(f)$ is the Fourier transform of $g(t)$. $S_a(f)$ and $S_J(f)$ denote the power spectral density of $a(t)$ and $J(t)$, respectively. Note that the accurate expressions for $S_a(f)$ and $S_J(f)$ are not

$$\begin{aligned}
\sigma_J &= \frac{1}{4\pi}\sqrt{(D_1 + D_{-1} + D_2)} \quad (24)\\
D_1 &= \frac{f_s\{PP_1(0) - |P_1(2f_s)|\cos(\vartheta_1 - 2\theta_1)\}}{8B_1^2}\\
D_{-1} &= \frac{f_s\{PP_{-1}(0) - |P_{-1}(-2f_s)|\cos(\vartheta_{-1} + 2\theta_{-1})\}}{8B_{-1}^2}\\
D_2 &= \frac{f_s\{|PQ(0)|\cos(\varphi_q - \theta_1 + \theta_{-1}) - |PG(2f_s)|\cos(\varphi_G - \theta_1 - \theta_{-1})\}}{4B_1B_{-1}}
\end{aligned}$$

available, but the relationship between $S_a(f)$ and σ_A, as well as $S_J(f)$ and σ_J, is given by

$$\sigma_A = \sqrt{\langle a^2(t)\rangle} = \sqrt{\int_{-\infty}^{\infty} S_a(f)\,df} \tag{27}$$

$$\sigma_J = f_s\sqrt{\int_{-\infty}^{\infty} S_J(f)\,df}. \tag{28}$$

On the other hand, the power spectral density of $I_c(t)$ can be calculated using the frequency transfer function of the FPF as shown in Appendix B. For convenience, we can use $S_I^c(f)$ and $\sum_{n=-\infty}^{\infty} S_I^d(nf_s)\delta(f-nf_s)$ to represent continuous power spectral density component and the discrete power spectral density components of $S_I(f)$, respectively. Then we get

$$\begin{aligned} &S_I^c(f) + \sum_{n=-\infty}^{\infty} S_I^d(nf_s)\delta(f-nf_s) \\ &\quad\cong f_s^2 \sum_{n=-\infty}^{\infty} |G(nf_s)|^2 \\ &\qquad\cdot \left[S_a(f-nf_s) + 4\pi^2 n^2 f_s^2 S_J(f-nf_s) + \delta(f-nf_s)\right]. \end{aligned} \tag{29}$$

Integrating (29), and combining (27) and (28), we obtain

$$\sigma_A = \sqrt{\frac{\displaystyle\int_{-\infty}^{\infty} S_I^c(f)\,df - \sum_{n=-\infty}^{\infty} 4\pi^2 n^2 \sigma_J^2 S_I^d(nf_s)}{\displaystyle\sum_{n=-\infty}^{\infty} S_I^d(nf_s)}}. \tag{30}$$

It is easily seen that as long as the value of σ_J [can be achieved from (24)] and the expression for $S_I(f)$ (shown in Appendix B) are known, we can get the value of σ_A.

IV. Numerical Results and Discussion

To numerically investigate the timing performance in such an optical tank circuit, we assume that the incoming optical data pulses have Gaussian profiles

$$u(t) = \exp\left(-\frac{(1+jC)}{2}\,\frac{t^2}{T_0^2}\right) \tag{31}$$

where C is the linear chirp parameter and T_0 is the half-width at the $1/e$ point. In this paper, we take $T_0 = T_s/(6\sqrt{In(2)})$, corresponding to 1/3 of slot width (FWHM).

A. The Impacts of Finesse of the FPF

We denote F as the finesse of the FPF, which is given by $\pi\sqrt{R}/(1-R)$ (7). Fig. 3 gives the calculated σ_A as a function of F for ideal clock extraction, where the solid line and dashed line denote the calculated results using time-domain and frequency-domain methods, respectively. It can be observed that the two theories agree very well. In our calculations using frequency-domain method, to save computational time, some amplitude noise spectra are neglected. So the results obtained by the frequency-domain method exhibit a little lower than that obtained by the time-domain method. From Fig. 3, we can find that σ_A decreases as F increases, and σ_A can be less than 0.1 if F is greater than 600. This is due to the fact that F is equivalent to the quality factor in a conventional electrical tank circuit. It is obvious that an FPF with a greater F can perform better in noise suppression.

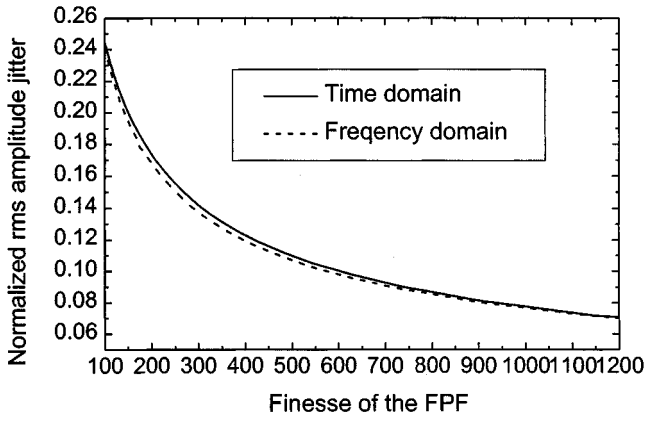

Fig. 3. σ_A versus F for ideal clock extraction.

B. The Impacts of Carrier Frequency Drift

From Fig. 1, we can find that when the carrier frequency deviates from the ideal setting, the line spectral components of the extracted optical clock decreases, but the noise component (corresponding to the continuous spectral component inside the passband of the FPF) increases. It is immediate that the introduction of carrier frequency drift Δf will degrade the jitter performance and also reduce the average optical clock power (denoted as $\overline{I}_c$ hereafter). Such results are clearly shown in Fig. 4(a) and (b), where we have neglected the impacts of resonator detuning and carrier phase noise. We used the time-domain method in our calculations. Note that Fig. 4 only gives the results for $\Delta f > 0$, since the case of $\Delta f < 0$ gives same results. From Fig. 4, we can observe that a very small value of Δf can result in a significant increase in σ_A and decrease in $\overline{I}_c$. Moreover, it can be found that the greater the value of F, the more serious the degradation. For example, if we choose $F = 600$, when $\Delta f = 0, 0.001 f_s$, and $0.005 f_s$, the corresponding σ_A becomes 0.095, 0.12, and 0.32, and the normalized $\overline{I}_c$ becomes 1, 0.4, and 0.04, respectively. If we need $\sigma_A < 0.1$, Δf must be controlled to be less than 0.001 f_s. Typically for $f_s = 100$ GHz, $\Delta f < 100$ MHz is then required. Currently such a requirement is still impracticable. Note that $\overline{I}_c$ is strongly dependent on Δf; therefore a feedback control can be introduced in such an optical tank circuit (simply using $\overline{I}_c$ as the feedback signal) to make the FSR of the Fabry–Perot resonator follow the variation of f_0 and hence keep f_0 always a multiple of FSR. In this case, however, resonator detuning becomes inevitable. A more practical design is to introduce both feedback control (at the receiver) and carrier frequency control (at the transmitter). Under such a design, the requirement for carrier frequency controls is dependent on the

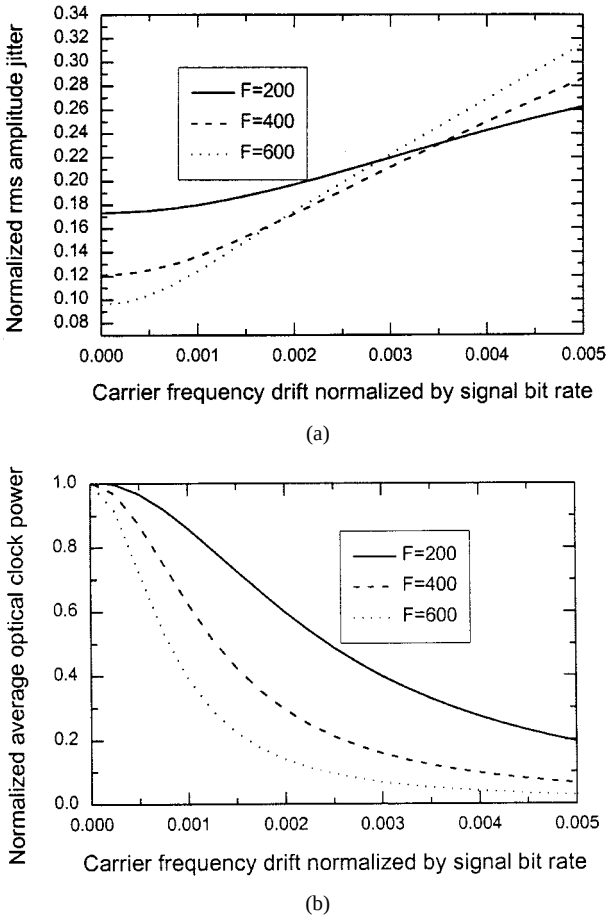

Fig. 4. Impacts of carrier frequency drift on (a) rms amplitude jitter and (b) average optical clock power for the case that $T_R = T_s$ and $\delta f = 0$.

tolerance to the resonator detuning. Assuming that the acceptable maximum resonator detuning is given by $df_{\max}$, we then need to control Δf to be less than $f_0 df_{\max}/\mathrm{FSR}$.

C. The Impacts of Resonator Detuning

From Section II, we know that when FSR$\neq f_s$, both amplitude jitter and phase jitter will occur in the extracted clock. In this case, frequency-domain method needs to be used to investigate the timing performance. Fig. 5(a)–(c) gives the calculated results, where we have assumed that $F = 600$, $\Delta f = 0$, and $C = 0$. Apart from degrading both σ_A and σ_J, it can be observed that resonator detuning df also introduces an extra phase shift in the extracted optical clock. It is worth noting that such a phase shift goes up very quickly as df increases. Typically, for the case of $F = 600$, when $df = 0.0001 f_s$, $0.0002 f_s$, and $0.0004 f_s$, the resulted extra phase shift is estimated to be 0.1, 0.22, and 0.45 rad, respectively.

From Fig. 5(b) and (c), we can see that the impact of resonator detuning on σ_J is much greater than that on σ_A. A very small resonator detuning can result in a large increase in the value of σ_J. Moreover, the greater the finesse of the FPF is, the more serious such a degradation becomes. For the case of $F = 600$, when $df = 0.0001 f_s$, $0.0002 f_s$, and $0.0004 f_s$, the corresponding σ_J is estimated to be 0.018, 0.035, and 0.063, respectively. On the contrary, the influence of resonator detuning

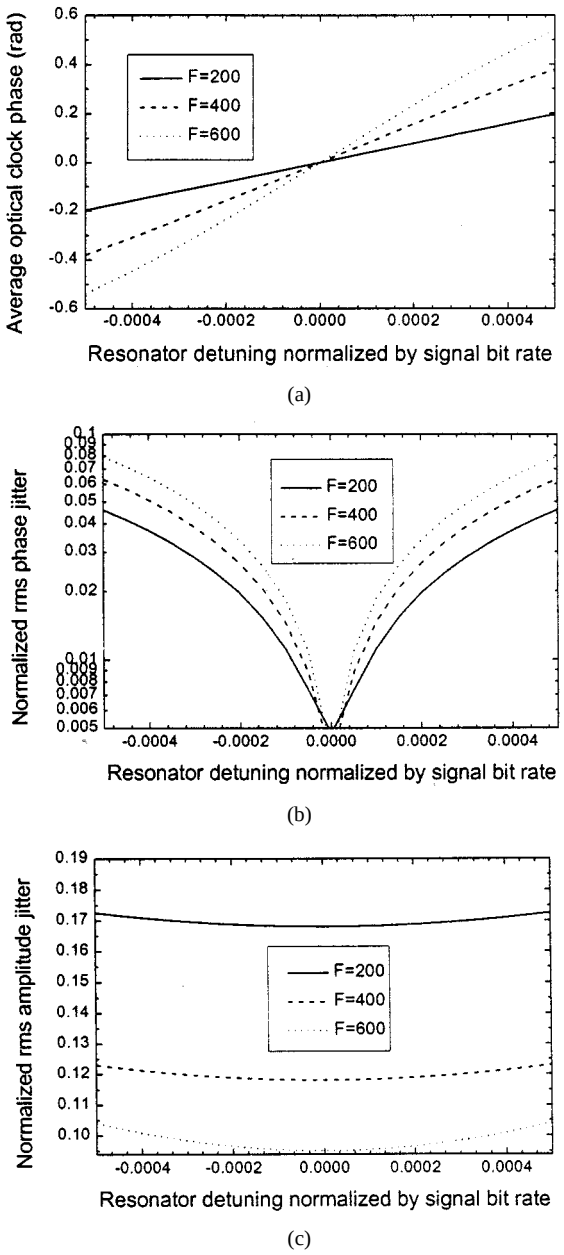

Fig. 5. Impacts of resonator detuning on (a) average optical clock phase, (b) rms phase jitter, and (c) rms amplitude jitter of the extracted optical clock for the case that $\Delta f = 0$, $\delta f = 0$, and $C = 0$.

on σ_A remains small for various values of F. This can be explained as follows.

Observing (26) carefully, we can find that in the extracted optical clock, the amplitude-noise sidebands predominate at the harmonics of sufficiently low order. The phase-noise sidebands have power proportional to n^2 and predominate for harmonics of higher order. From Fig. 1, it can be easily seen that the impact of resonator detuning on harmonics of higher order is more severe than that of lower order. It is then immediate that resonator detuning degrades σ_J more severe than σ_A. Since the clock power mainly focuses on the harmonics of low order, it can be supposed that the impact of resonator detuning on $\overline{I}_c$ is relatively small. This is verified by our calculation. For $F = 600$, when $df = 0.0001 f_s$, $0.0002 f_s$, and $0.0004 f_s$, the normalized $\overline{I}_c$ is 0.99, 0.97, and 0.92, respectively.

TABLE I
TIMING PERFORMANCE UNDER OPTICAL CARRIER FREQUENCY STABILITY SPECIALIZED BY ITU-T G. 692 FOR THE CASE THAT $F = 600$ AND $\delta f = 0$

Carrier frequency drift	5 GHz	11 GHz	23 GHz
σ_J	0.006	0.01	0.02
σ_A	0.0955	0.0960	0.0965
Extra phase shift (rad.)	0.025	0.056	0.12

Note that resonator detuning is mainly introduced by slowly varying carrier frequency drift when a feedback control suggested above is utilized. The introduction of extra phase shift implies that the average phase of the extracted optical clock will fluctuate with the carrier frequency. For practical clock extraction, if we require the maximum extra phase shift less than 0.1 rad, $\sigma_J < 0.02$ and $\sigma_A < 0.1$, $F = 600$ and $df < 0.0001 f_s$ are necessary. This implies that $\Delta f < 20$ GHz (1.55 μm band) is required. Such a frequency stabilization technology is available in a wavelength-division-multiplexing (WDM) system. According to ITU-T standards (G.692), for a 2.5 Gbit/s system with unequally spaced channel frequency allocation, when the frequency slot is 25, 50, and 100 GHz, the allowable maximum center frequency deviations are $\pm$4–5 GHz, $\pm$11 GHz, and $\pm$23 GHz, respectively. Table I gives the corresponding timing performance for the case that $F = 600$ and $\delta f = 0$ in 1.55-μm band.

D. The Impacts of Carrier Phase Noise

Now we investigate the influence of carrier phase noise through time-domain method. The results are given in Fig. 6 ($\Delta f = 0$ and $df = 0$ are assumed). It is worth noting that the introduction of carrier phase noise does not degrade σ_A. On the contrary, σ_A reduces as δf goes up. For example, in the case where $F = 600$, when $\delta f = 0$, $0.01 f_s$, and $0.04 f_s$, σ_A is given by 0.1, 0.085, and 0.074, respectively. However, from the view of $\overline{I}_c$, $\delta f = 0$ is the best choice, since $\overline{I}_c$ decreases rapidly as δf increases. For the case that $F = 600$ and $\delta f = 0.04 f_s$, the normalized $\overline{I}_c$ is estimated to be 0.03.

From the time-domain analysis shown in Section II [see (3)], we can find that the optical clock pulse can be viewed as a sum (in field form) of a series of successive pulses multiplied by their individual reflective factor R^k. The introduction of optical phase noise can degrade the coherence between these pulses and decrease the probabilities for constructive interference. As a result, the amplitude fluctuation of the extracted optical clock pulse is reduced. It is clear that $\overline{I}_c$ will reduce accordingly. In fact, when the incoming optical pulses are incoherent, i.e., carrier phase noise is very large, we can get the minimum value of σ_A as $\sqrt{1 - R^2/(1 + R^2)}$ ($\Delta f = 0$ and $df = 0$ are assumed). For $F = 600$, σ_A is given by 0.071.

E. The Impacts of Optical Pulse Chirp

In conventional RZ systems, optical pulse chirp can be introduced by optical signal source and nonlinear effects such as self-phase modulation (SPM) and cross-phase modulation (XPM) during transmission. So it is important to investigate their impacts on the optical tank circuit.

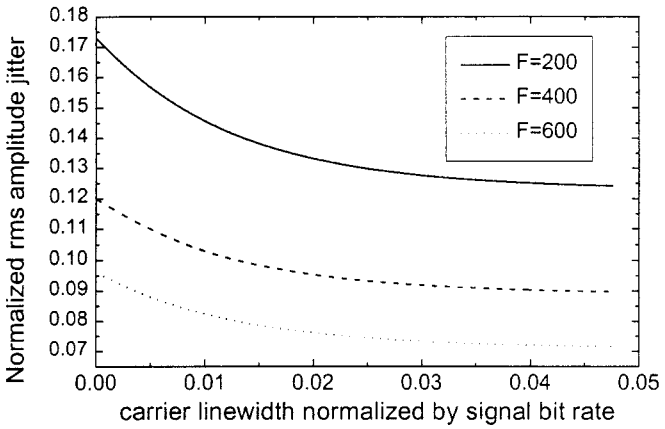

(a)

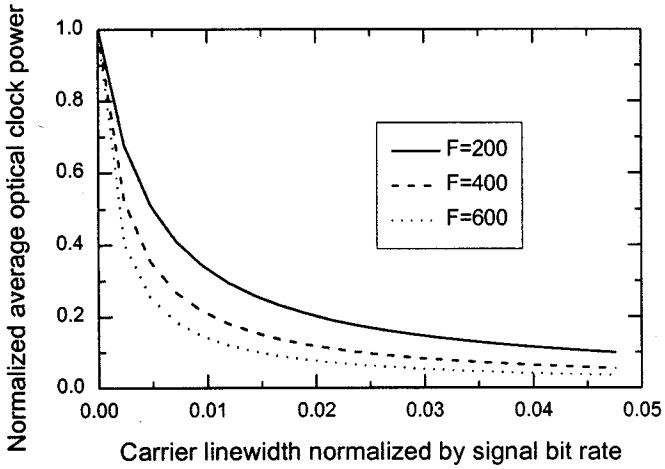

(b)

Fig. 6. Impacts of carrier phase noise on (a) rms amplitude jitter and (b) average optical clock power for the case that $\Delta f = 0$ and $df = 0$.

From (3) and (31), we can get the field of the extracted optical clock in the interval $[nT_s, (n+1)T_s]$ as

$$e_0(t)|_{nT_s} = T \sum_{k=0}^{\infty} a_{n-k} |u(t - nT_s - kdt)| \cdot \exp\left(-\frac{jC(t - nT_s - kdt)^2}{2T_0^2}\right) R^k \cdot e^{j2\pi f_c (t - kT_R) + \phi(t - kT_R)} \tag{32}$$

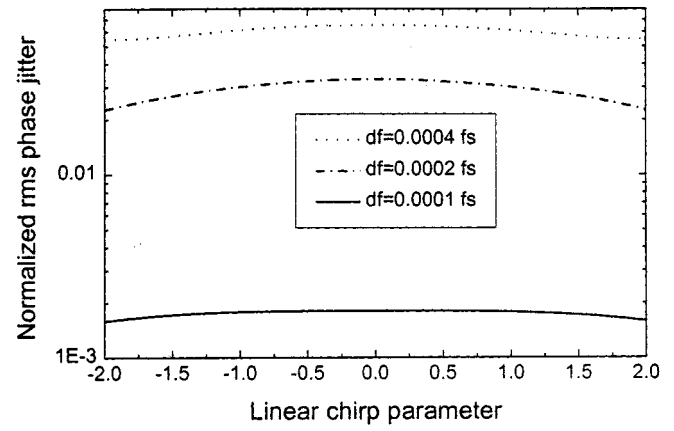

(a)

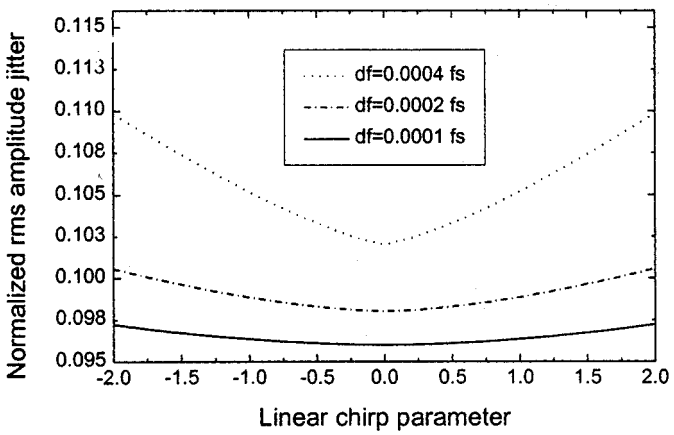

(b)

Fig. 7. Impacts of optical pulse frequency chirp on (a) rms phase jitter and (b) rms amplitude jitter for the case that $\Delta f = 0$ and $\delta f = 0$.

where $dt = -df/\mathrm{FSR}f_s$ and C is linear chirp parameter. If $df = 0$, we can see that the introduction of optical pulse chirp does not impose any impact on the timing performance. In the case where $df \neq 0$, its impact is dependent on the value of df. Fig. 7(a) and (b) gives the calculated results using the proposed frequency-domain method. Though the introduction of optical pulse chirp will degrade σ_A, we can see that such a degradation becomes serious only when the value of df is relatively large. From the above discussion, we know that the allowable df should be less than $0.0001f_s$. In this case, the influence of optical pulse chirp on σ_A is small even when $C = \pm 2$. For the case of phase jitter, the introduction of chirp can slightly lower the value of σ_J, as is shown in Fig. 7(b).

Our calculation also shows that the introduction of optical pulse chirp will lead to a decrease in $\overline{I}_c$. However, it is found that as long as $df < 0.0001f_s$ and $|C| < 2$, the influence of optical pulse chirp remains small (the normalized $\overline{I}_c$ can be more than 0.96).

F. Application in Multiwavelength Clock Extraction

From the above discussions, we can see that the passive optical tank circuit based on FPF cannot eliminate the chirp in the extracted optical clock pulses. Therefore, such a clock extraction technique is unsuitable for a regenerative repeater. However, due to its simplicity, this technique may be advantageous to use for synchronization in future all-optical time-division switching systems [15]–[18] (bit optical clock are necessary for both optical buffer and optical circulating shift register). Incorporating an all-optical circulating shift register and an AND gate, this circuit is also suitable for frame synchronization in an optical time-division-multiplexed (OTDM) demultiplexer similar to the case of electrical TDM demultiplexer. Moreover, the passive optical tank circuit can be used for multiwavelength clock recovery, which is especially desirable in systems that apply WDM technology. An active optical tank circuit based on SBS is also suitable for multiwavelength clock extraction; however, the allowable wavelength span is limited by the inherent pump detuning (about 3 nm) [10], [11]. In the following, we will show that for a passive optical tank circuit based on FPF, the allowable wavelength span is nearly unlimited.

We consider the case where there is a total of n RZ optical data streams with the same bit rate (bit clock is f_s). We use f_1, $f_2, \ldots$ and f_n to denote their individual carrier frequency. Then we can see that as long as we have $f_1 = q_1 f_s$, $f_2 = q_2 f_s$, …, $f_n = q_n f_s$ (q_1, q_2, …, q_n are integers), and f_s =FSR, the n clocks can be recovered through only one FPF. In principle, it can be seen that the number of n is unlimited.

For multiwavelength clock extraction, the requirements for carrier frequency controls become more stringent. If a feedback control is introduced in the optical tank circuit (to lock any one of the carriers to one of the power transmission peaks of the FPF), the absolute carrier frequency variations of less than 20 GHz ($\sim$0.155 μm, 1.55 μm band) and relative frequency variations of less than $0.001f_s$ are needed then. To achieve this, a possible method is to use a single supercontinuum (SC) as the multiwavelength optical source. To construct large flexible optical networks, and utilize both OTDM and WDM technologies, SC broad-band optical source has received much attention in recent years [19]–[24].

An SC broad-band optical source usually consists of a high coherent short-pulse optical source, an optical amplifier, a section of SC fiber, and a section of chirp compensation fiber. SC is explained as a complex nonlinear process due to the combined effect of SPM, XPM, four-wave mixing, and stimulated Raman scattering [23] induced by intense optical pump pulse. The generated spectra generally extend to both longer and shorter wavelengths from the pump wavelength and can exhibit an almost flat profile by choosing appropriate experimental conditions. Thus, multiwavelength transform-limited short pulses can easily be selected by filtering with passive optical filter.

For a stable SC broad-band source, the optical frequency stability of the filtered channels is determined by the used filtering devices. For conventional arrayed-waveguide grating (AWG), the absolute frequency stability was measured to be $\sim$1 GHz/°C, and the relative frequency stability can be better than 10^{-4}/°C [20]. If the temperature variation is controlled to be less than 0.4 °C, the absolute frequency stability of $\sim$400 MHz and relative frequency stability of better than 100 MHz over 20 nm bandwidth (1.55 μm band) are achievable.

To stabilize the SC spectral profile, we need to control the pump wavelength and pump pulse intensity and use relatively short SC fiber length [24]. For our multiwavelength clock ex-

TABLE II
A BRIEF COMPARISON FOR SEVERAL MAJOR ALL-OPTICAL CLOCK EXTRACTION TECHNIQUES. SOA: SEMICONDUCTOR OPTICAL AMPLIFIER

Clock recovery techniques	mode-locked fiber ring laser	mode-locked semiconductor laser	Optical PLL	Optical passive tank circuit	Optical active tank circuit
Clock pulse quality	Transform-limited	Transform-limited	Transform-limited	Dependent on data pulse	Dependent on data pulse
Complexity	High	high	Very high	low	High
Operational speed (in principle)	>100 Gbit/s	Limited by gain recovery time of SOA [25]	> 100 Gbit/s	> 1Tbit/s	> 100 Gbit/s
Long-term stability	Difficult	Achievable	Achievable	Achievable	Achievable
Multi-wavelength clock extraction	No	No	No	Yes	Yes
Bit rate transparent	No	No	No	No	Yes

traction, from the view of the worst case, absolute frequency variation of the pump optical pulse needs to be less than 20 GHz ($\sim$0.155 μm, 1.55 μm band). Since the SC spectra are approximately flat, the allowable pump light frequency drift in fact can be larger.

Finally, a brief comparison for several major all-optical clock recovery techniques is shown in Table II.

V. CONCLUSIONS

We have analytically investigated the timing performance in an optical tank circuit based on FPF. Time-domain analysis has shown that there is no phase jitter in the extracted optical clock if the FSR of the FPF is exactly equal to the incoming signal clock frequency. Based on this, an analytical expression for rms amplitude jitter is obtained in time domain, where we have taken carrier frequency drift and carrier phase noise into account. When the FSR of the FPF deviates from the signal clock frequency, both amplitude jitter and phase jitter will occur in the extracted optical clock. To investigate the timing performance at this situation, we develop a more general frequency-domain method. This method is also suitable for other optical tank circuits, such as that based on SBS [11], and allows us to calculate both rms phase jitter and rms amplitude jitter of the extracted optical clock. Using the two developed methods, we numerically investigate the impacts of the finesse of the resonator, carrier frequency drift, laser phase noise, and resonator detuning on the timing performance in such an optical clock extraction circuit. Finally, application of this circuit in multiwavelength clock recovery was discussed.

APPENDIX A

From (8), $\langle |b_m(t)|^4 \rangle$ can be given as

$$\langle |b_m(t)|^4 \rangle = \sum_{k_1=-\infty}^{\infty} \sum_{k_2=-\infty}^{\infty} \sum_{k_3=-\infty}^{\infty} \sum_{k_4=-\infty}^{\infty} \cdot \langle a_{k1} a_{k2} a_{k3} a_{k4} \rangle T^4 R^{k_1+k_2+k_3+k_4} \cdot e^{a[|k_1-k_2|+|k_3-k_4|]+jb[k_1-k_2+k_3-k_4]}. \quad \text{(A1)}$$

For convenience, we use $\Lambda(R, T)_{k_1, k_2, k_3, k_4}$ to represent

$$\sum_{k_1=-\infty}^{\infty} \sum_{k_2=-\infty}^{\infty} \sum_{k_3=-\infty}^{\infty} \sum_{k_4=-\infty}^{\infty} T^4 R^{k_1+k_2+k_3+k_4} \cdot e^{a[|k_1-k_2|+|k_3-k_4|]+jb[k_1-k_2+k_3-k_4]}.$$

Then $\langle |b_m(t)|^4 \rangle$ can be expressed as

$$\begin{aligned}
\langle |b_m(t)|^4 \rangle &= \tfrac{1}{16} \underbrace{\Lambda(R, T)_{k_1, k_2, k_3, k_4}}_{k_1 \neq k_2 \neq k_3 \neq k_4} \\
&\quad + \tfrac{1}{8} \underbrace{\Lambda(R, T)_{k_1, k_2, k_3, k_4}}_{\text{Three of } k_1, k_2, k_3 \text{ and } k_4 \text{ are unequal}} \\
&\quad + \tfrac{1}{4} \underbrace{\Lambda(R, T)_{k_1, k_2, k_3, k_4}}_{\text{Two of } k_1, k_2, k_3 \text{ and } k_4 \text{ are unequal}} \\
&\quad + \tfrac{1}{2} \Lambda(R, T)_{k_1, k_1, k_1, k_1} \\
&= \tfrac{1}{16} \Lambda(R, T)_{k_1, k_2, k_3, k_4} \\
&\quad + \tfrac{1}{16} \{\Lambda(R, T)_{k_1, k_1, k_3, k_4} \\
&\qquad + \Lambda(R, T)_{k_1, k_2, k_1, k_4} \\
&\qquad + \Lambda(R, T)_{k_1, k_2, k_3, k_1} \\
&\qquad + \Lambda(R, T)_{k_1, k_2, k_2, k_4} \\
&\qquad + \Lambda(R, T)_{k_1, k_2, k_3, k_2} \\
&\qquad + \Lambda(R, T)_{k_1, k_2, k_3, k_3}\} \\
&\quad + \tfrac{1}{16} \{\Lambda(R, T)_{k_1, k_1, k_2, k_2} \\
&\qquad + \Lambda(R, T)_{k_1, k_2, k_1, k_2} \\
&\qquad + \Lambda(R, T)_{k_1, k_2, k_2, k_1} \\
&\quad - \tfrac{1}{8} \Lambda(R, T)_{k_1, k_1, k_1, k_1}. \quad \text{(A2)}
\end{aligned}$$

Note that $\Lambda(R, T)_{k_1, k_1, k_3, k_4} = \Lambda(R, T)_{k_1, k_2, k_3, k_3}$ and $\Lambda(R, T)_{k_1, k_2, k_2, k_4} = \Lambda(R, T)_{k_1, k_2, k_3, k_1}$. Through tedious mathematical deduction, $\langle |b_m(t)|^4 \rangle$ is finally given the form as in (12).

APPENDIX B

According to classical Weiner theorem [26], the power spectral density of $I_c(t)$ can be expressed as

$$S_I(f) = FT_\tau\left[\frac{1}{T_s}\int_{-(T_s/2)}^{T_s/2} R_{I,I}(t,\tau)\,dt\right]. \qquad \text{(B1)}$$

In (B1), $R_{I,I}(t,\tau)$ is the autocorrelation function of $I_c(t)$ and $FT_\tau[\,]$ is the Fourier transform. Assuming $\eta = f/f_s$, and using the results of (A1) and (A2), we can get $S_I(f)$ as

$$\begin{aligned} S_I(\eta f_s) = {} & \frac{f_s^4}{16}\sum_{k_1=-\infty}^{\infty} \\ & \cdot\left\{\sum_{k_2=-\infty}^{\infty}\sum_{k_3=-\infty}^{\infty} Y(k_2,k_1)Y(k_3,-k_1)\right. \\ & \quad + \sum_{k_2=-\infty}^{\infty}\Psi(-k_1)[Y(k_2,-k_1)+Y(k_2,k_1)] \\ & \quad \left. + \Psi(k_1)\Psi(-k_1)\right\}\delta(\eta-k_1) \\ & + \frac{f_s^3}{16}\sum_{k_1=-\infty}^{\infty}\sum_{k_2=-\infty}^{\infty}\{Y^*(k_2-\eta,k_1)Y(k_2,k_1) \\ & \qquad + Y(k_2+\eta,k_1)Y^*(k_2,k_1) \\ & \qquad + Y^*(-k_2,-\eta)Y^*(k_1+k_2,\eta) \\ & \qquad + Y(-k_2,\eta)Y(k_1+k_2,-\eta)\} \\ & + \frac{f_s^3}{16}\sum_{k_1=-\infty}^{\infty}[\Theta_1(\eta,k_1)+\Theta_1(-k_1,\eta)] \\ & - \frac{f_s^3}{8}\Psi^2(-\eta) \end{aligned} \qquad \text{(B2)}$$

where

$$\begin{aligned} Q(\eta) &= U(\eta f_s)H(\eta f_s), \\ Y(\eta_1,\eta_2) &= Q(\eta_1)Q^*(\eta_2+\eta_1), \\ \Psi(\eta) &= \int_{-\infty}^{\infty} Y(\eta',\eta)\,d\eta', \\ \Theta_1(\eta_1,\eta_2) &= \int_{-\infty}^{\infty} Y(\eta',\eta_1)Y(\eta_2-\eta',-\eta_1)\,d\eta' \\ \Theta_2(\eta_1,\eta_2) &= \int_{-\infty}^{\infty} Y(\eta',\eta_1)Y^*(\eta_2+\eta',-\eta_1)\,d\eta'. \end{aligned}$$

REFERENCES

[1] L. Adams, E. Kintzer, and J. Fujimoto, "All-optical clock recovery using a mode-locked figure eight laser with a semiconductor nonlinearity," *Electron. Lett.*, vol. 30, p. 1696, Sept. 1994.

[2] R. Ludwig, "10 GHz all-optical clock recovery using a mode locked semiconductor laser in a 40 Gb/s, 100 km transmission experiment," in *Proc. OFC'96*, Mar. 1996, pp. 131–132.

[3] A. Ellis, K. Smith, and D. Patrick, "All-optical clock recovery at bit rates up to 40 Gbit/s," *Electron. Lett.*, vol. 29, pp. 1741–1743, Sept. 1993.

[4] S. Kawanishi and M. Saruwatari, "Ultrahigh-speed PLL-type clock recovery circuit based on all-optical gain modulation in travelling-wave laser diode amplifier as a 50 GHz detector," *Electron. Lett.*, vol. 29, pp. 1714–1715, Sept. 1993.

[5] O. Kamatani and S. Kawanishi, "Ultrahigh-speed clock recovery with phase lock loop based on four-wave mixing in a traveling-wave laser diode amplifier," *J. Lightwave Technol.*, vol. 14, pp. 1757–1767, Aug. 1996.

[6] M. Jinno, T. Matsumoto, and M. Koga, "All-optical timing extraction using an optical tank circuit," *IEEE Photon. Technol. Lett.*, vol. 2, pp. 203–204, Feb. 1990.

[7] M. Jinno and T. Matsumoto, "Optical tank circuit used for all-optical timing recovery," *J. Quantum Electron.*, vol. 28, pp. 895–900, Apr. 1992.

[8] H. Kawakami, Y. Miyamoto, T. Kataoka, and K. Hagimoto, "All-optical timing clock extraction using multiple wavelength pumped Brillouin amplifier," *IEICE Trans. Commun.*, vol. E78-B, pp. 694–700, May 1995.

[9] D. L. Butler, J. S. Wey, M. W. Chbat, G. L. Burdge, and J. Goldhar, "Optical clock recovery from a data stream of an arbitrary bit rate by use of stimulated Brillouin scattering," *Opt. Lett.*, vol. 20, no. 6, pp. 560–562, June 1995.

[10] C. Johnson, K. Demarest, C. Allen, R. Hui, K. V. Peddanarappagari, and B. Zhu, "Multi-wavelength all-optical clock recovery," *IEEE Photon. Technol. Lett.*, vol. 11, pp. 895–897, July 1999.

[11] X. Zhou, H. H. M. Shalaby, L. Chao, T. H. Cheng, and P. Ye, "A performance analysis of all-optical clock extraction circuit based on stimulated Brillouin scattering," *J. Lightwave Technol.*, vol. 18, pp. 1453–1466, Oct. 2000.

[12] J. A. Armstrong, "Theory of interferometer analysis of laser noise," *J. Optic. Soc. Amer.*, vol. 56, pp. 1024–1031, Aug. 1966.

[13] M. J. W. Rodwell, D. M. Bloom, and K. J. Weingarten, "Subpicosecond laser timing stabilization," *IEEE J. Quantum Electron.*, vol. 25, pp. 817–827, Apr. 1989.

[14] D. A. Leep and D. A. Holm, "Spectral measurement of timing jitter in gain-switched semiconductor lasers," *Appl. Physics. Lett.*, vol. 60, pp. 2451–2453, Oct. 1992.

[15] K. L. Hall, "40 Gbit/s optical packet buffering," in *Proc. OFC*, Mar. 1997, ThD3.

[16] M. Kalyvas, C. Bintjas, K. Houbavlis, H. Avramopoulos, L. Occhi, L. Schares, G. Guekos, S. Hansmann, and R. Dall'Ara, "All-optical write/read memory for 20 Gbit/s data packets," *Electron. Lett.*, vol. 36, no. 12, pp. 1050–1051, June 2000.

[17] D. K. Hunter and D. G. Smith, "New architecture for optical TDM switching," *J. Lightwave Technol.*, vol. 11, pp. 495–511, Mar. 1993.

[18] H. J. Lee and H. G. Kim, "Polarisatin- independent all-optical circulating shift register based on self-phase modulation of semiconductor optical amplifier," *Electron. Lett.*, vol. 35, pp. 170–171, Jan. 1999.

[19] T. Morioka, H. Takara, S. Kawanishi, O. Kamatani, K. Takiguchi, K. Uchiyama, M. Saruwatari, H. Takahashi, M. Yamada, T. Kanamori, and H. Ono, "1 Tbit/s (100 Gbit/s '10 Channel) OTDM/WDM transmission using a single supercontinuum WDM source," *Electron. Lett.*, vol. 32, pp. 906–907, May 1996.

[20] T. Morioka, K. Uchiyama, S. Kawanishi, S. Suzuki, and M. Saruwatari, "Multi-wavelength picosecond pulse source with low jitter and high optical frequency stability based on 200 nm supercontinuum filtering," *Electron. Lett.*, vol. 31, pp. 1064–1065, June 1995.

[21] S. Kawanishi, H. Takara, T. Morioka, O. Kamatani, and M. Saruwatari, "200 Gbit/s, 100 km time-division-multiplexed optical transmission uisng supercontinuum pulses with prescaled PLL timing extraction and all-optical demultiplexer," *Electron. Lett.*, vol. 31, pp. 816–817, May 1995.

[22] S. Accheo and L. Boivin, "Investigation and design rules of supercontinuum sources for WDM applications," *Proc. OFC*, vol. 3, pp. 2–4, Mar. 2000.

[23] R. R. Alfano, *Supercontinuum Laser Source*. Heidelberg: Springer-Verlag, 1989.

[24] G. A. Nowak, J. Kim, and M. N. Islam, "Stable 200 nm TDM/WDM source based on continuum generation in 2 m of fiber," in *Proc. OFC*, Mar. 1999, TuB3-1.

[25] Mathason and P. J. Delfyett, "Pulsed injected locking dynamics of passively mode-locked external-cavity semiconductor laser systems for all-optical clock recovery," *J. Lightwave Technol.*, vol. 18, pp. 1111–1120, Aug. 2000.

[26] A. Buchwald and K. W. Martin, *Integated Fiber-Optic Receiver*. New York: Kluwer Academic, 1995, pp. 27–103.

Xiang Zhou (M'00) was born in China. He received the B.Sc. degree in applied physics from Shanghai Fudan University, China, in 1991 and the Ph.D. degree in optical fiber communication from Beijing University of Posts & Telecommunications, China, in 1999.

He was with the Chinese Institute of Engineering Physics as an Assistant Researcher for three years. Currently he is with Nanyang Technological University as a Research Fellow, working on technologies for wide-band optical amplifier, optical clock extraction, and photonic IP routing.

Chao Lu (M'91), photograph and biography not available at the time of publication.

Ping Shum (M'00), photograph and biography not available at the time of publication.

Hossam H. M. Shalaby (S'83–M'91–SM'99), photograph and biography not available at the time of publication.

T. H. Cheng (M'00), photograph and biography not available at the time of publication.

Peida Ye (SM'85–F'88) is Honorary President of Beijing University of Posts and Telecommunications (BUPT), China. He is a Senior Academician of the Chinese Academy of Science and a Chief Scientist with the National Information Office.